Applied Physics Letters

Bipolar conductivity in ferroelectric La:HfZrO films

Cite as: Appl. Phys. Lett. **118**, 262903 (2021); https://doi.org/10.1063/5.0050748
Submitted: 18 March 2021 . Accepted: 17 June 2021 . Published Online: 02 July 2021

Timofey V. Perevalov, Andrei A. Gismatulin, Vladimir A. Gritsenko, Igor' P. Prosvirin, Furqan Mehmood, Thomas Mikolajick, and Uwe Schroeder

Applied Physics Letters ARTICLE scitation.org/journal/apl

Bipolar conductivity in ferroelectric La:HfZrO films

Cite as: Appl. Phys. Lett. **118**, 262903 (2021); doi: 10.1063/5.0050748
Submitted: 18 March 2021 · Accepted: 17 June 2021 ·
Published Online: 2 July 2021

Timofey V. Perevalov,[1,2,a)] Andrei A. Gismatulin,[1] Vladimir A. Gritsenko,[1,2,3] Igor' P. Prosvirin,[4] Furqan Mehmood,[5] Thomas Mikolajick,[5,6] and Uwe Schroeder[5]

AFFILIATIONS

[1]Rzhanov Institute of Semiconductor Physics SB RAS, 13 Lavrentiev Ave., 630090 Novosibirsk, Russia
[2]Novosibirsk State University, 2 Pirogov Str., 630090 Novosibirsk, Russia
[3]Novosibirsk State Technical University, 20 Marx Ave., 630073 Novosibirsk, Russia
[4]Boreskov Institute of Catalysis SB RAS, 5 Lavrentiev Ave., 630090 Novosibirsk, Russia
[5]NaMLab gGmbH, Noethnitzer Str., 64 a, 01187 Dresden, Germany
[6]Chair of Nanoelectronics, TU Dresden, 01062 Dresden, Germany

[a)]**Author to whom correspondence should be addressed:** timson@isp.nsc.ru

ABSTRACT

Lanthanum-doped HfZrO is considered as the ferroelectric material for capacitor structures used in one-transistor-one capacitor nonvolatile memory cells for the development of new generation nonvolatile random-access memory. Here, different capacitor structures are characterized by x-ray photoelectron spectroscopy electrically to determine the electron and hole contribution to the conductivity in these capacitor structures. Experiments related to the minority carrier's injection and charge transport from an *n*-Si and a *p*-Si substrate into a lanthanum-doped HfZrO layer show that the conductivity is bipolar. Electrons are injected into La:HfZrO from a negatively biased contact, and accordingly, holes are injected from a positive voltage biased electrode.

Ferroelectric random-access memory (FeRAM) is one of the possible promising candidates to realize a random-access memory that is nonvolatile.[1] However, modern FeRAM devices are limited in scaling and cannot compete with dynamic random-access memories (DRAM) in terms of their density and cost.[2] The discovery of ferroelectricity in hafnium oxide solves the basic scaling issue of FeRAM devices.[3] However, due to the high coercive field in ferroelectric hafnium oxide, the maximum number of read/write cycles here is currently in the range of 10^{10} or even below, which is the orders of magnitude below the requirement of a virtually unlimited endurance.[4] It was shown that the ferroelectric hafnium oxide endurance is correlated with the leakage current and, thus, with the charge injection, transport, and defect generation, finally leading to a ferroelectric breakdown.[5] The exact origin of the degradation mechanisms determines the lifetime of ferroelectric capacitors and is still a subject of scientific investigations. However, the La doping was shown to increase the cycling endurance of $Hf_{0.5}Zr_{0.5}O_2$ (HfZrO) films.[4,6] Therefore, the charge transport mechanism in La doped HfZrO films is particularly interesting to understand the starting point for the degradation mechanisms.

Normally, the dielectric film conduction is assumed to be monopolar and, in most cases, electron conduction is dominant. However, in contrast, it was shown that Si_3N_4, HfO_2, GeO_2, TiO_2, and ZrO_2 can also have a two-band conduction, i.e., the conduction is determined by both electrons and holes.[7–13] The charge carrier's sign in a semiconductor can be verified by measuring the Hall effect. However, this method is not applicable for dielectrics due to the very low free charge carrier's concentration. The charge carrier's sign in dielectrics can be determined by the minority carrier's injection from an *n*-type and *p*-type silicon substrate into metal-insulator-semiconductor (MIS) structures.[7–13] The electron and hole contribution to the dielectric conductivity also depends on the configuration of the MIS structure. So the conductivity of Si_3N_4 in the metal-nitride-oxide-silicon structure with tunnel thin SiO_2 is bipolar,[8,14] whereas it with thick SiO_2 is monopolar (electronic).[8] The dielectric conductivity in the $Al/HfO_2/Si$ structure at both polarities is monopolar (electronic)[15] but in the $Ni/HfO_2/Si$ structure is two-band, bipolar.[12]

The purpose of this paper is the determination of electron and hole contribution to the conductivity in ferroelectric $La:Hf_{0.5}Zr_{0.5}O_2$ in the Si/La:HfZrO/TiN/Ti/Pt structure.

First, a metal-ferroelectric-insulator-semiconductor (MFIS) and metal-ferroelectric-metal (MFM) capacitors were fabricated by the atomic layer deposition of ferroelectric La-doped HfZrO layers on silicon or on TiN on a silicon substrate. Tetrakis(ethylmethylamino)hafnium

{Hf[N(C_2H_5)CH_3]$_4$}, tetrakis[ethylmethylamino]zirconium {Zr[N(C_2H_5)CH_3]$_4$}, and tris(isopropyl-cyclopentadienyl)lanthanum [La-(iPrCp)$_3$] were used for deposition at 280 °C in the Oxford Instruments OPAL system as hafnium, zirconium, and lanthanum precursors, respectively. Oxygen plasma was used as an oxidant for La, while H_2O was utilized for Hf and Zr Atomic layer deposition (ALD) cycles. La doped $Hf_{0.5}Zr_{0.5}O_2$ was deposited by alternating HfO_2 and ZrO_2 ALD cycles with one additional LaO_x ALD cycle based sub-monolayers every 22 $Hf_{0.5}Zr_{0.5}O_2$ layers up to an overall thickness of about 20 nm. A 12 nm thick titanium nitride top electrode was deposited at room temperature similar to the bottom electrode using a sputtering system from Alliance Concept. The samples were then annealed at 500 °C for 1 min in the N_2 atmosphere. The La concentration of approximately 3.5% was calculated from the corresponding growth rate values and cycle ratios. Since La_2O_3 was always deposited on a $Hf_{0.5}Zr_{0.5}O_2$ underlayer, it is likely that the real composition is proportional to the calculated values. Since only a small amount of the La_2O_3 interlayer is introduced in the $Hf_{0.5}Zr_{0.5}O_2$ layer and the La atoms are not uniformly distributed in the $Hf_{0.5}Zr_{0.5}O_2$ layer, a structural characterization method would not be able to determine a more precise La content. La is assumed to be substitutional in the $Hf_{0.5}Zr_{0.5}O_2$ lattice. To pattern the capacitor structures, a 10 nm thick titanium layer was deposited as an adhesion layer and 25 nm thick platinum was deposited by the electron beam evaporation through a shadow mask. The wet chemical etching of the TiN top electrode was carried out for patterning using 5% NH_3 and 2% H_2O_2 solutions in H_2O at the temperature of 50 °C (by SC1 etching). The silicon substrate resistance was 7.5 Ω·cm for both *n*-Si and *p*-Si substrates. In the further reading, the $Hf_{0.5}Zr_{0.5}O_2$ film doped with about 3.5 mol. % La is abbreviated as La:HfZrO.

The x-ray photoelectron spectra (XPS) were measured on a SPECS spectrometer using a PHOIBOS-150 MCD-9 analyzer and FOCUS-500 monochromator (Al Kα radiation, $h\nu = 1486.74$ eV, 200 W). The binding energy (BE) scale was pre-calibrated using the Au $4f_{7/2}$ (BE = 84.0 eV) and Cu $2p_{3/2}$ (BE = 932.67 eV) core level peak positions. The peaks binding energy was set based on the C1*s* peak (BE = 284.8 eV) position, which corresponds to the hydrocarbon-like deposits on the surface. Shirley method was used for the background subtraction. A convolution of Gaussian and Lorentz functions was used to fit the core peaks.

The current–voltage (*I*–*V*) sweep measurements were performed on the prepared structures in the temperature range from 300 to 400 K in a Linkam LTS420E cell using a Keithley 2400 and Linkam T95 temperature controller. The voltage ramp rate applied for the *I*–*V* measurement was 0.9 V/s. The capacitance–voltage (*C*–*V*) measurements were characterized utilizing the Agilent E4980A equipment connected to the probe station.

First, the x-ray photoelectron spectra (XPS) were measured on La-doped HfZrO films. The Hf4*f* and Zr3*d* levels can be well approximated by single doublets with the Hf $4f_{7/2}$ and Zr $3d_{5/2}$ peaks of 17.0 eV and 182.3 eV, respectively [Figs. 1(a) and 1(b)]. These positions correspond to the Hf_4^+ and Zr_4^+ states for stoichiometric HfO_2[16,17] and ZrO_2.[18,19] The La $3d_{5/2}$ level shows the main peak at the energy of 834.1 eV and the corresponding satellite at 836.8 eV [Fig. 1(c)]. The energy agrees very well to the corresponding spectrum from the previous studies of La_2O_3.[20] The presence of the satellite is determined by the shakeup process in which electrons are promoted

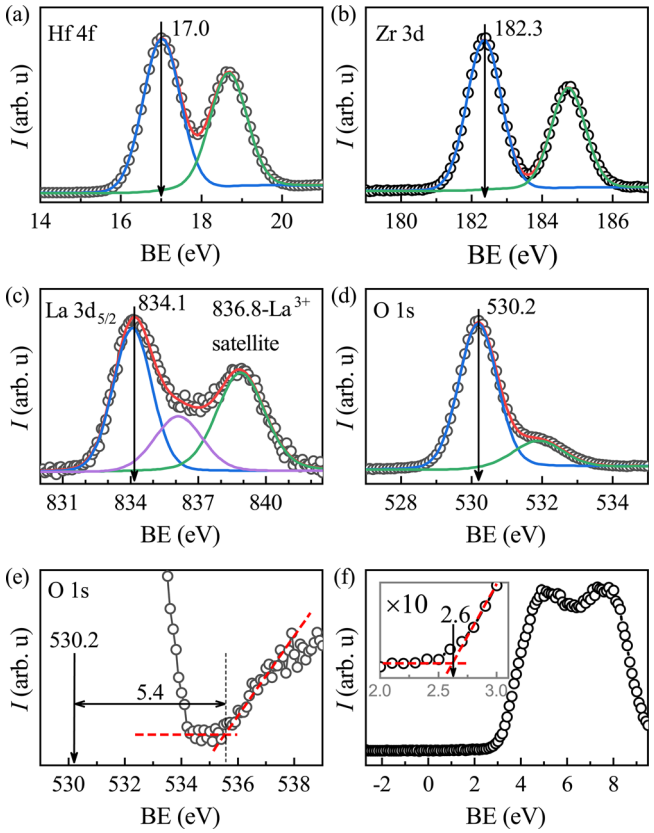

FIG. 1. XPS of the La:HfZrO film (symbols) and deconvolution (lines) of Hf4*f* (a), Zr3*d* (b), La $3d_{5/2}$ (c) and O1*s* (d) levels. (e) The bandgap estimation from the O1*s* photoelectron energy loss spectra. (f) Valence band XPS and determination of the valence band top position.

from the filled O^{2-} 2*p* to empty La^{3+} 4*f* levels.[21,22] Thus, the La atoms in the La-doped HfZrO layer are, predominantly, in the La_2O_3 composition. The O1*s* XPS decays into two peaks, the first of which with the maximum energy of 530.2 eV can be unambiguously assigned to the lattice oxygen in the mixture of HfZrO. The second peak with the maximum energy of 531.8 eV is characteristic for weakly bound adsorbed oxygen on the samples surface [Fig. 1(d)]. The O1*s*-XPS also reflects the photoelectron energy loss spectrum for the excitation of inter-band electron transitions from the valence band to the conduction band. It allows the bandgap energy value E_g estimation. E_g is determined by the linear interpolation of the edge of the excitation spectrum from inter-band transitions to the background level [Fig. 1(e)]. The estimation of the E_g value yields 5.4 ± 0.2 eV. This result is consistent with the value of 5.37 eV previously determined for $Hf_{0.5}Zr_{0.5}O_2$ from the transmission spectra.[23]

The valence band XPS is used to determine the valence band top (E_V) position relative to the level of an electron in vacuum for the studied films [Fig. 1(f)]. Since the valence band top state's binding energy is 2.6 eV and the absolute zero of the used spectrometer, found from the binding energy of the Au4*f* level, Fermi edge, and the Au work function, is 5.0 eV, which is relative to the vacuum level, the absolute E_V position is 7.6 eV. The justification for this approach is a fact that

La incorporation suppresses the Fermi level pinning (FLP) effect.[24,25] So the vacuum energies of Au and La:HfZrO are aligned. Moreover, our result is consistent with the corresponding data for HfO_2 and ZrO_2.[26] Knowing this value as well as the E_V position relative to the vacuum level for Si (5.2 eV[27]) and the electron work function for TiN (4.5 eV[28]), one can construct an energy diagram for the Si/La:HfZrO/TiN structure (see the insets in Fig. 2). These simplified diagrams illustrate the two-band conductivity and do not consider the localization of electrons and holes in the dielectric, as well as the SiO_x layer on the Si substrate is presented.

The measurement of the current–voltage curve on the *p*-Si/La:HfZrO/TiN/Ti/Pt capacitor structure with two bias polarities on the metal is shown in Fig. 2(a). When the voltage at the top metal electrode is positive in the depletion mode, the current saturation is observed in the dark. The current value is increased when the illumination is turned on. The saturation is associated with the minority charge carrier's injection in this case, electrons, from Si into the dielectric. Thus, the current in the dielectric is provided by the electrons injected from Si. When the potential at the metal is negative in the accumulation mode, the current is increased exponentially with the voltage rise and the illumination has no effect on the current value. Almost, all of the applied voltage drops across the dielectric.

For the *n*-Si/La:HfZrO/TiN/Ti/Pt structure, the current is increased when the illumination is turned on in the depletion mode if a negative potential is applied to the metal and does not change in the accumulation mode with a positive potential on the metal [Fig. 2(b)]. Thus, when a negative potential is applied to the metal, the current in the dielectric is caused by the holes injected from Si. Accordingly, it can be concluded that the La:HfZrO film conductivity is bipolar.

The electron and hole injection from Si into La:HfZrO can be determined by the sign of the accumulated charge in the dielectric based on the capacitance–voltage characteristic. When a positive potential is applied to the metal for a structure on the *n*-Si substrate, the *C*–*V* characteristic shifts to the right, indicating the negative charge accumulation from the electrons localized on the traps in the dielectric [Fig. 3(a)]. This indicates the electron injection from *n*-Si in the

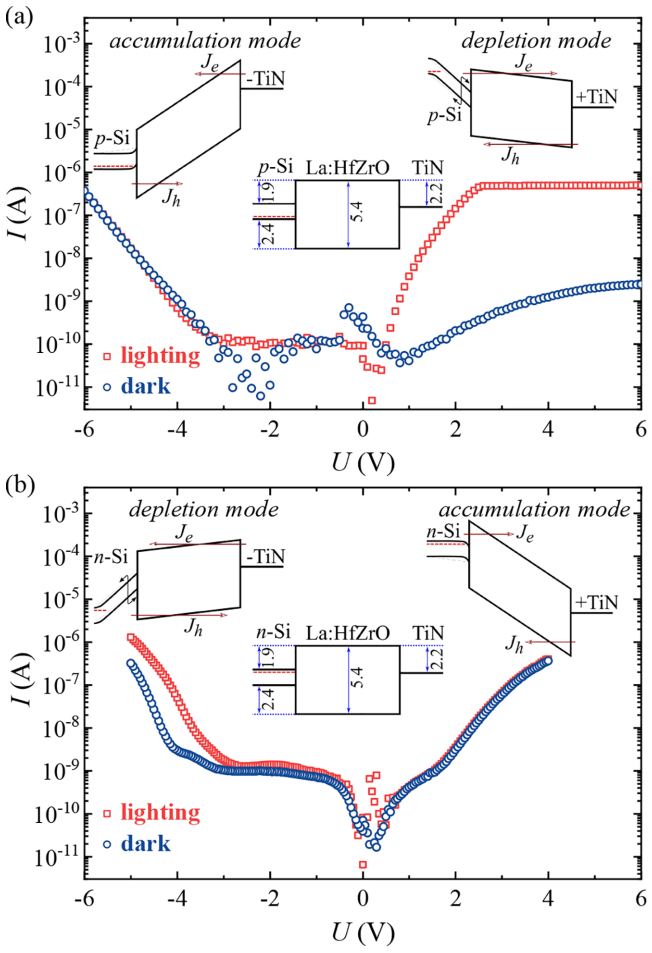

FIG. 2. Current–voltage characteristics of *p*-Si/La:HfZrO/TiN (a) and *n*-Si/La:HfZrO/TiN (b) structures in the dark and under illumination. The insertions presents the relevant energy diagrams of *p*-Si/La:HfZrO/TiN and *n*-Si/La:HfZrO/TiN structures without applied voltage, in the depletion mode, and in the accumulation mode.

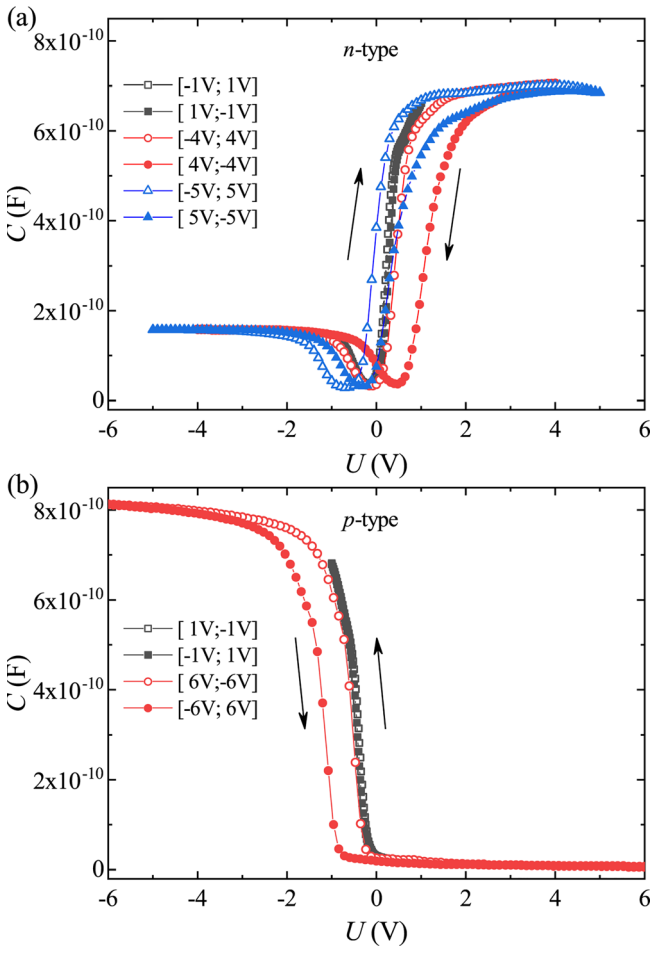

FIG. 3. Capacitance–voltage characteristics of *n*-Si/La:HfZrO/TiN (a) and *p*-Si/La:HfZrO/TiN (b) structures.

accumulation mode. When a negative potential is applied to the metal for the structure with *p*-Si, the *C*–*V* characteristic shifts to the left [Fig. 3(b)]. This indicates the accumulation of a positive charge from the holes localized on the traps in La:HfZrO. This suggests the hole injection from *p*-Si in the accumulation mode. Thus, the hysteresis of the *C*–*V* characteristic independently confirms that the La:HfZrO conductivity is bipolar. For a positive potential on the metal electrode, electrons from the Si substrate are injected into the dielectric, and for a negative potential on the metal, holes from the Si substrate are introduced in the dielectric layer. Previously, the bipolar conductivity was observed also for pure HfO_2[12] and ZrO_2 films.[13] Here, we confirm that HfZrO, even when doped with La, will still conduct both electrons and holes.

In summary, the energy diagram of the Si/La:HfZrO/TiN structure was constructed from the photoelectron spectroscopy data. The saturation current in the depletion mode in the *n*-Si/La:HfZrO/TiN and *p*-Si/La:HfZrO/TiN structures and an increase in the current level in the accumulation mode under illumination indicate the minority charge carrier's injection from the silicon substrate into the adjacent dielectric. In the accumulation mode, the majority charge carrier injection and accumulation are observed in both structures. Thus, the La:HfZrO conductivity is bipolar and two-band. Electrons are injected into the dielectric from a negatively biased contact, and correspondingly, holes are injected for a positively applied voltage.

This work was supported by the Russian Foundation for Basic Research, Grant No. 20-57-12003 (*I*–*V*, *C*–*V* measurements), and under the state contract with ISP SBRAS No. 0242-2021-0003 (XPS). F.M. received a partial funding from the European Union Horizon 2020 research and the innovation programme under grant agreement No. 780302. Parts of this work were funded by DFG Grant No. 430054035.

DATA AVAILABILITY

The data that support the findings of this study are available within the article.

REFERENCES

[1]T. Schenk, M. Pesic, S. Slesazeck, U. Schroeder, and T. Mikolajick, Rep. Prog. Phys. **83**(8), 086501 (2020).
[2]H. P. McAdams, R. Acklin, T. Blake, X. H. Du, J. Eliason, J. Fong, W. F. Kraus, D. Liu, S. Madan, T. Moise, S. Natarajan, N. Qian, Y. C. Qiu, K. A. Remack, J. Rodriguez, J. Roscher, A. Seshadri, and S. R. Summerfelt, IEEE J. Solid-St. Circ. **39**(4), 667–677 (2004).
[3]T. Mikolajick, U. Schroeder, and S. Slesazeck, IEEE Trans. Electron Dev. **67**(4), 1434–1443 (2020).
[4]A. G. Chernikova, M. G. Kozodaev, D. V. Negrov, E. V. Korostylev, M. H. Park, U. Schroeder, C. S. Hwang, and A. M. Markeev, ACS Appl. Mater. Inter. **10**(3), 2701–2708 (2018).
[5]D. R. Islamov, V. A. Gritsenko, T. V. Perevalov, V. A. Pustovarov, O. M. Orlov, A. G. Chernikova, A. M. Markeev, S. Slesazeck, U. Schroeder, T. Mikolajick, and G. Y. Krasnikov, Acta Mater. **166**, 47–55 (2019).
[6]F. Mehmood, M. Hoffmann, P. D. Lomenzo, C. Richter, M. Materano, T. Mikolajick, and U. Schroeder, Adv. Mater. Interfaces **6**(21), 1901180 (2019).
[7]F. H. Hielscher and H. M. Preier, Solid-State Electron. **12**(7), 527–538 (1969).
[8]V. A. Gritsenko and E. E. Meerson, Phys. Stat. Sol. A Appl. Res. **62**(2), K131–K134 (1980).
[9]Z. A. Weinberg, Solid-State Electron. **20**(1), 11–18 (1977).
[10]D. R. Islamov, V. A. Gritsenko, C. H. Cheng, and A. Chin, Appl. Phys. Lett. **103**(23), 232904 (2013).
[11]D. R. Islamov, V. A. Gritsenko, C. H. Cheng, and A. Chin, Appl. Phys. Lett. **101**(3), 032101 (2012).
[12]D. R. Islamov, V. A. Gritsenko, C. H. Cheng, and A. Chin, Appl. Phys. Lett. **99**(7), 072109 (2011).
[13]D. R. Islamov, V. A. Gritsenko, T. V. Perevalov, V. S. Aliev, V. A. Nadolinny, and A. Chin, Materialia **15**, 100980 (2021).
[14]K. A. Nasyrov, V. A. Gritsenko, Y. N. Novikov, E. H. Lee, S. Y. Yoon, and C. W. Kim, J. Appl. Phys. **96**(8), 4293–4296 (2004).
[15]S. Shaimeev, V. Gritsenko, K. Kukli, H. Wong, E. H. Lee, and C. Kim, Microelectron. Rel. **47**(1), 36–40 (2007).
[16]O. Renault, D. Samour, J. F. Damlencourt, D. Blin, F. Martin, S. Marthon, N. T. Barrett, and P. Besson, Appl. Phys. Lett. **81**(19), 3627–3629 (2002).
[17]R. Jiang, E. Q. Xie, and Z. F. Wang, Appl. Phys. Lett. **89**(14), 142907 (2006).
[18]T. S. Jeon, J. M. White, and D. L. Kwong, Appl. Phys. Lett. **78**(3), 368–370 (2001).
[19]S. Tsunekawa, K. Asami, S. Ito, M. Yashima, and T. Sugimoto, Appl. Surf. Sci. **252**(5), 1651–1656 (2005).
[20]C. V. Ramana, R. S. Vemuri, V. V. Kaichev, V. A. Kochubey, A. A. Saraev, and V. V. Atuchin, ACS Appl. Mater. Interfaces **3**(11), 4370–4373 (2011).
[21]P. Burroughs, A. Hamnett, A. F. Orchard, and G. Thornton, J. Chem. Soc. Dalton **1976**, 1686–1698.
[22]M. F. Sunding, K. Hadidi, S. Diplas, O. M. Lovvik, T. E. Norby, and A. E. Gunnaes, J. Electron Spectrosc. Related Phenom. **184**(7), 399–409 (2011).
[23]F. Ambriz-Vargas, G. Kolhatkar, R. Thomas, R. Nouar, A. Sarkissian, C. Gomez-Yanez, M. A. Gauthier, and A. Ruediger, Appl. Phys. Lett. **110**(9), 093106 (2017).
[24]X. P. Wang, M. F. Li, A. Chin, C. X. Zhu, J. Shao, W. Lu, X. C. Shen, X. F. Yu, R. Chi, C. Shen, A. C. H. Huan, J. S. Pan, A. Y. Du, P. Lo, D. S. H. Chan, and D. L. Kwong, Solid-State Electron. **50**, 986–991 (2006).
[25]X. P. Wang, C. Shen, M. Li, H. Y. Yu, Y. Sun, Y. P. Feng, A. Lim, H. W. Sik, A. Chin, Y. C. Yeo, P. Lo, and D. L. Kwong, in Technical Digest of VLSI Symposium (2006), Vol. 12.
[26]V. V. Afanas'ev, *Internal Photoemission Spectroscopy: Principles and Applications* (Elsevier Science, 2008), p. 312.
[27]D. T. Pierce and W. E. Spicer, Phys. Rev. B **5**, 3017–3029 (1972).
[28]S. A. Vitale, J. Kedzierski, P. Healey, P. W. Wyatt, and C. L. Keast, IEEE Trans. Electron. Dev. **58**(2), 419–426 (2011).